COMPDYN 2015
5th ECCOMAS Thematic Conference on
Computational Methods in Structural Dynamics and Earthquake Engineering
M. Papadrakakis, V. Papadopoulos, V. Plevris (eds.)
Crete Island, Greece, 25–27 May 2015

TOPOPLOGY OPTIMIZATION OF TWO-DIMENSIONAL WAVE BARRIERS FOR THE REDUCTION OF GROUND VIBRATION TRANSMISSION

Cédric Van hoorickx[1], Ole Sigmund[2], Mattias Schevenels[3], Boyan S. Lazarov[2], and Geert Lombaert[1]

[1]KU Leuven, Department of Civil Engineering, Structural Mechanics Section
Kasteelpark Arenberg 40, 3001 Leuven, Belgium
e-mail: {cedric.vanhoorickx, geert.lombaert}@bwk.kuleuven.be

[2]DTU, Department of Mechanical Engineering, Solid Mechanics
Nils Koppels Allé, Building 404, 2800 Lyngby, Denmark
e-mail: {sigmund, bsl}@mek.dtu.dk

[3]KU Leuven, Department of Architecture, Architectural Engineering
Kasteelpark Arenberg 1, 3001 Leuven, Belgium
e-mail: mattias.schevenels@asro.kuleuven.be

Keywords: Topology optimization, Elastodynamic wave propagation, Vibration reduction measures, Wave barriers

Abstract. *This paper studies topology optimization as a tool for designing barriers for ground vibration transmission. A two-dimensional problem is considered where material is stiffened in the design domain, located in the transmission path between the wource and the receiver. The two-dimensional homogeneous halfspace is excited at the surface. The response at the receiver is minimized for a harmonic load by distributing a stiffened material in the design domain using topology optimization. The performance is compared to a wall barrier which has the same volume of material and has a depth equal to the depth of the design domain. At low frequencies, where the wavelengths are large compared to the height of the domain, the optimized wave barrier reflects and guides waves away from the surface. At high frequencies, destructive interference is obtained that leads to high values of the insertion loss. The presence of small features in the designs makes the performance sensitive to deviations in the geometry. In order to obtain a design which is robust with respect to geometric imperfections, a worst case approach is followed. The resulting design not only outperforms the wall barrier, but is also robust with respect to deviations in the geometry. This paper also shows that the robust design can be used to develop simplified design solutions.*

1 INTRODUCTION

Vibrations in the built environment are a matter of growing concern. Railway induced vibrations may lead to malfunctioning of sensitive equipment, discomfort to people and, at high vibration levels, damage to structures. Furthermore, noise can be re-radiated from floors and walls when local modes are excited. More and more research is performed to search for efficient and cost-effective vibration mitigation measures. Three categories of mitigation measures can be distinguished: at the source (the railway track) [1], on the transmission path (the ground) [2], and at the receiver (the building) [3]. The present work considers wave barriers to hinder propagation of ground vibration from source to receiver.

Until now, only a limited number of simple design geometries for mitigation measures has been investigated. However, current flexibility in construction methods such as jet grouting leaves much room for improvement. To discover novel design geometries, topology optimization [4] is applied. Topology optimization was originally developed for static mechanical problems, but has since then been used for a variety of applications including problems governed by wave propagation. Topology optimization has been applied to problems with electromagnetic (photonic crystal waveguide designs [5]), elastodynamic (design of phononic band-gap materials and structures [6]), and acoustic waves (noise barriers [7, 8]). In this study, topology optimization is used to develop novel design geometries for barriers impeding elastodynamic wave transmission.

Since structural optimization is often found to lead to designs which are very sensitive to geometrical imperfections [9], a worst case approach is adopted where the worst performance of some (extreme) cases is optimized. This paper demonstrates the importance of considering robustness in the optimization process, and shows that the robust designs can be used to develop simplified design solutions.

The paper is organized as follows. First, the optimization problem is introduced and the topology optimization approach is briefly presented. Second, results for optimized wave barriers are discussed. Third, robust topology optimization is applied to obtain designs less sensitive to geometric imperfections and a simplified design is presented.

2 THE OPTIMIZATION PROBLEM

Figure 1 shows the considered optimization problem. A two-dimensional homogeneous elastic halfspace is considered which is excited at the surface by a vertical harmonic load.

The goal is to minimize the response at an output point (the receiver), located at the surface of the halfspace, at a distance of $15\,\mathrm{m}$ from the excitation point. The effectiveness of the wave barrier is quantified by the insertion loss (IL) in this output point:

$$\mathrm{IL} = 20 \log \left(\frac{\left| \hat{u}_{\mathrm{out}}^{\mathrm{orig}} \right|}{|\hat{u}_{\mathrm{out}}|} \right) \tag{1}$$

with $\left| \hat{u}_{\mathrm{out}}^{\mathrm{orig}} \right|$ the norm of the displacement vector in the output point in the case of the original homogeneous halfspace without the wave barrier and $|\hat{u}_{\mathrm{out}}|$ the norm of the displacement vector in the case with wave barrier.

The displacements are obtained using the finite element method with two-dimensional four-node elements in plane strain. An element size of $0.25\,\mathrm{m}$ is used for the mesh, corresponding to ten elements per shear wavelength λ_s at a frequency of $80\,\mathrm{Hz}$, which is the upper limit considered in this work. At the boundaries of the finite element mesh, appropriate radiation boundary

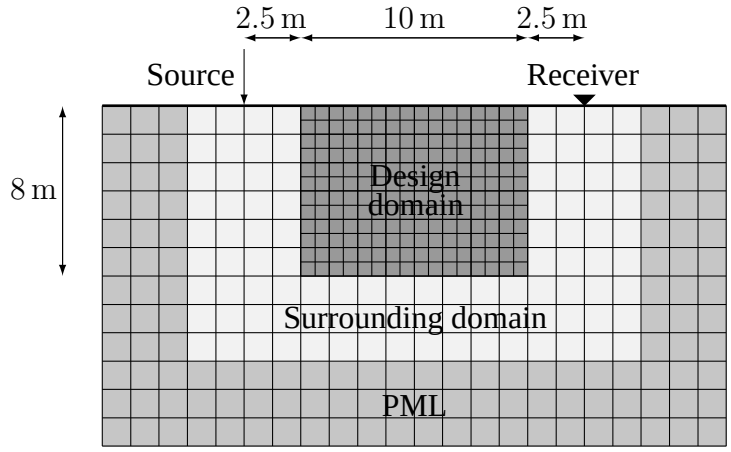

Figure 1: The considered optimization problem.

conditions have to prevent spurious wave reflections. The Perfectly Matched Layers (PML) of Harari and Albocher [10] are applied. The resulting finite element equilibrium equations can be written as:

$$\hat{\mathbf{K}}\hat{\mathbf{u}} = \hat{\mathbf{p}} \tag{2}$$

where $\hat{\mathbf{p}}$ is the load vector, $\hat{\mathbf{u}}$ is the displacement vector, and $\hat{\mathbf{K}}$ is the dynamic stiffness matrix.

The material is stiffened in a design domain which is located between the source and the receiver. The design domain has a cross-sectional area of $10 \times 8\,\mathrm{m}^2$ and is located at a distance of $2.5\,\mathrm{m}$ from both the excitation point and the receiver. The properties of the original material 1 of the homogeneous halfspace and the stiffened material 2 are summarized in table 1.

Property	Original material 1	Stiffened material 2
Material density ρ	$2000\,\mathrm{kg/m^3}$	$2000\,\mathrm{kg/m^3}$
Longitudinal wave velocity C_p	$400\,\mathrm{m/s}$	$950\,\mathrm{m/s}$
Shear wave velocity C_s	$200\,\mathrm{m/s}$	$550\,\mathrm{m/s}$

Table 1: The considered material properties.

The optimal distribution of the stiffened material in the design domain is determined using topology optimization [4]. The material distribution is parameterized using so-called element densities $\bar{\rho}_e$ for each element e in the design domain. The value $\bar{\rho}_e = 0$ indicates that element e has the properties of the homogeneous halfspace, while the value $\bar{\rho}_e = 1$ corresponds to the properties of the stiffened material. The densities are allowed to vary continuously between 0 and 1, making it possible to solve the optimization problem with a gradient based approach.

A Solid Isotropic Material with Penalization (SIMP) interpolation is used to interpolate the material properties α:

$$\alpha = \alpha_1 + \bar{\rho}_e^p \left(\alpha_2 - \alpha_1\right) \tag{3}$$

where α_1 and α_2 are the properties of the original and stiffened material, respectively. The penalization factor $p \geq 1$ avoids so-called gray designs with intermediate densities. A value

$p = 1$ is used for the material density ρ while $p = 3$ is used for the constrained modulus ρC_{p}^2 and the shear modulus ρC_{s}^2. Note that the penalization only works if the volume constraint in Eq. (6) is active.

In order to achieve a design with sufficient detail, the finite element mesh of the design domain is finer than the one of the surrounding domain, following the method proposed by Kristensen [11]. The horizontal and vertical displacements of the intermediate nodes are coupled to the nodes of the surrounding domain and the resulting constraint equations are added to the finite element equilibrium equations.

The (physical) element densities $\bar{\rho}_e$ are obtained from the design variables ρ_e of the optimization problem by applying a projection filter [12]:

$$\bar{\rho}_e = \frac{\tanh(\beta\eta) + \tanh(\beta(\tilde{\rho}_e - \eta))}{\tanh(\beta\eta) + \tanh(\beta(1-\eta))} \tag{4}$$

where β is a sharpness parameter, controlling the smoothness of the projection, η is the projection threshold, and the densities $\tilde{\rho}_e$ are obtained from:

$$\tilde{\rho}_e = \frac{\sum_{i=1}^{N} w_{ei} v_i \rho_i}{\sum_{i=1}^{N} w_{ei} v_i} \tag{5}$$

where v_i is the volume of element i and the weight $w_{ei} = \max(R - r_{ei})$ depends on the filter radius R and the center-to-center distance r_{ei} between the elements e and i. In the present work, the filter radius is taken to be $R = 2.5$ elements, the projection threshold value is set to $\eta = 0.5$ and the sharpness parameter β has an initial value equal to 1 and is doubled every 50 iterations until the value of 32 is reached.

The aim is to maximize the insertion loss in Eq. (1). The problem is reformulated as a minimization problem, by defining the objective function $\Phi = -\mathrm{IL}$. The optimization problem is also subjected to a volume constraint and can be summarized as:

$$\begin{aligned} \min_{\rho_e} \quad & \Phi = 20 \log \left(\frac{|\hat{u}_{\mathrm{out}}(\bar{\rho}_e)|}{\left|\hat{u}_{\mathrm{out}}^{\mathrm{orig}}\right|} \right) \\ \text{s.t.} \quad & \sum_{e=1}^{N} v_e \bar{\rho}_e \leq V^*, \quad e = 1 \ldots N \\ & 0 \leq \rho_e \leq 1, \qquad e = 1 \ldots N \end{aligned} \tag{6}$$

where N is the number of elements in the design domain and the upper limit for the volume V^* is set to 10% of the total volume. The displacements are computed using the finite element method. This problem is not convex, and multiple local minima may exist.

The optimization problem is solved using the method of moving asymptotes (MMA) [13]. This gradient-based approach necessitates the calculation of the derivatives of the objective function. To enable an efficient calculation of the sensitivities, the adjoint method is used (see, e.g. [4, p. 17]). The sensitivities are calculated as follows:

$$\frac{\partial \Phi}{\partial \bar{\rho}_e} = 2\mathrm{Re}\left\{ \boldsymbol{\lambda}^T \frac{\partial \hat{\mathbf{K}}}{\partial \bar{\rho}_e} \hat{\mathbf{u}} \right\} \tag{7}$$

where the vector $\boldsymbol{\lambda}$ is computed from the adjoint equation, which can be written in the following simplified form:

$$\hat{\mathbf{K}} \boldsymbol{\lambda} = -\frac{\partial \Phi}{\partial \hat{\mathbf{u}}} \tag{8}$$

3 TOPOLOGY OPTIMIZATION RESULTS

The wave designs obtained by topology optimization are compared with the reference design of a wall barrier which has the same volume of material and has a depth equal to the depth of the design domain: a rectangular design with dimensions $1\,\mathrm{m} \times 8\,\mathrm{m}$, located in the design domain at the side closest to the source. This reference design is shown in figure 2a. The optimization starts with an initial design where all element densities are assigned a value $\rho_e = 0.2$.

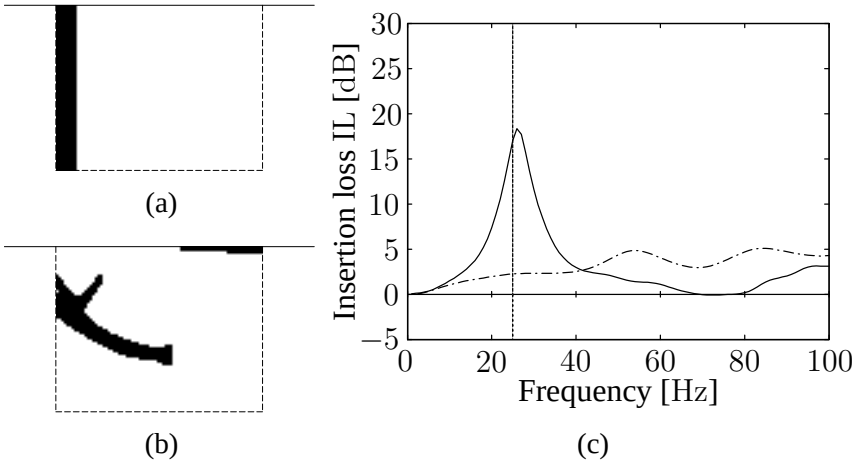

Figure 2: (a) Reference design, (b) optimized design maximizing the insertion loss at $25\,\mathrm{Hz}$, and (c) resulting insertion loss IL as a function of the frequency for the reference design (dash-dotted line) and the optimized design (solid line).

Maximizing the insertion loss in Eq. (1) for harmonic excitation at $25\,\mathrm{Hz}$ results in the design and corresponding insertion loss in figure 2. The optimized design leads to an insertion loss of $17.0\,\mathrm{dB}$ compared to the original situation which is $14.8\,\mathrm{dB}$ higher than the insertion loss of the reference design. Figure 3 shows the vector norm of the real and imaginary part of the displacement field at $25\,\mathrm{Hz}$ for the homogeneous halfspace and after the introduction of the reference barrier and the optimized barrier. The reference barrier mainly reflects the incoming waves and therefore reduces the amplitude of the Rayleigh waves travelling along the free surface from the source to the receiver. The optimized design, however, does not only reflect the incoming waves, but also directs them downwards into the soil, reducing the response at the surface.

The optimized design and its performance change significantly when the wavelength becomes smaller than the half of the depth of the design domain. Figure 4 shows the design and corresponding insertion loss when maximizing the insertion loss for harmonic excitation at $50\,\mathrm{Hz}$. The insertion loss of the optimized design is again compared to the insertion loss of the reference design of $1\,\mathrm{m} \times 8\,\mathrm{m}$. At $50\,\mathrm{Hz}$, the insertion loss reaches a very high value of $50.1\,\mathrm{dB}$, which is $45.7\,\mathrm{dB}$ higher than the insertion loss of the reference design. Figure 5 shows the vector norm of the real and imaginary part of the displacement field at $50\,\mathrm{Hz}$ for the homogeneous halfspace and after the introduction of the reference barrier and the optimized barrier. The reference barrier again primarily reduces the amplitude of the Rayleigh waves. The optimized design, however, moves the incoming waves away from the surface. This effect is caused by destructive interference of the waves transmitted by the top part of the optimized design and the waves reflected by the bottom part.

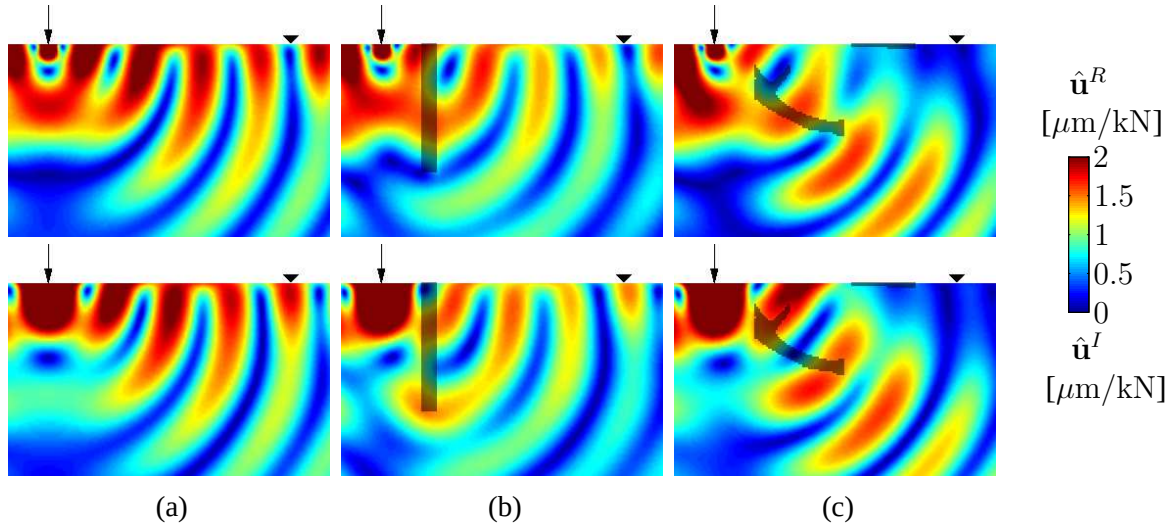

Figure 3: Vector norm of the real part $\hat{\mathbf{u}}^R$ (top) and imaginary part $\hat{\mathbf{u}}^I$ (bottom) of the displacement field at $25\,\mathrm{Hz}$ (a) for the homogeneous halfspace and after the introduction of (b) the reference design (figure 2a), and (c) the optimized design maximizing the insertion loss IL at $25\,\mathrm{Hz}$ (figure 2b).

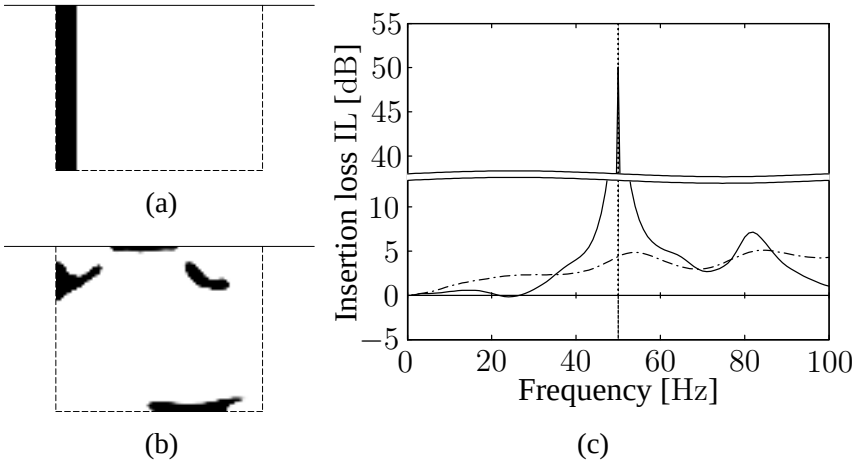

Figure 4: (a) Reference design, (b) optimized design maximizing the insertion loss at $50\,\mathrm{Hz}$, and (c) resulting insertion loss IL as a function of the frequency for the reference design (dash-dotted line) and the optimized design (solid line).

4 GEOMETRIC IMPERFECTIONS

The design in figure 4b contains some small features, making it very sensitive to deviations in the geometry. The performance of the actual wave barrier in case of geometric imperfections may therefore be far from optimal. The influence of errors in the (in-plane) dimensions of the stiffened material can be modeled by varying the projection threshold η in Eq. 4 [14].

Figure 6 shows the influence of the projection threshold η for the design optimized for reducing transmission at a frequency of $50\,\mathrm{Hz}$ (figure 4). For low values of the projection threshold (e.g. $\eta = 0.25$), lower values of the filtered densities are projected to the stiffened material as well, and the dimensions of the stiffened material increase, leading to so-called dilated designs. For high values of the projection threshold (e.g. $\eta = 0.75$), only the higher values of the filtered

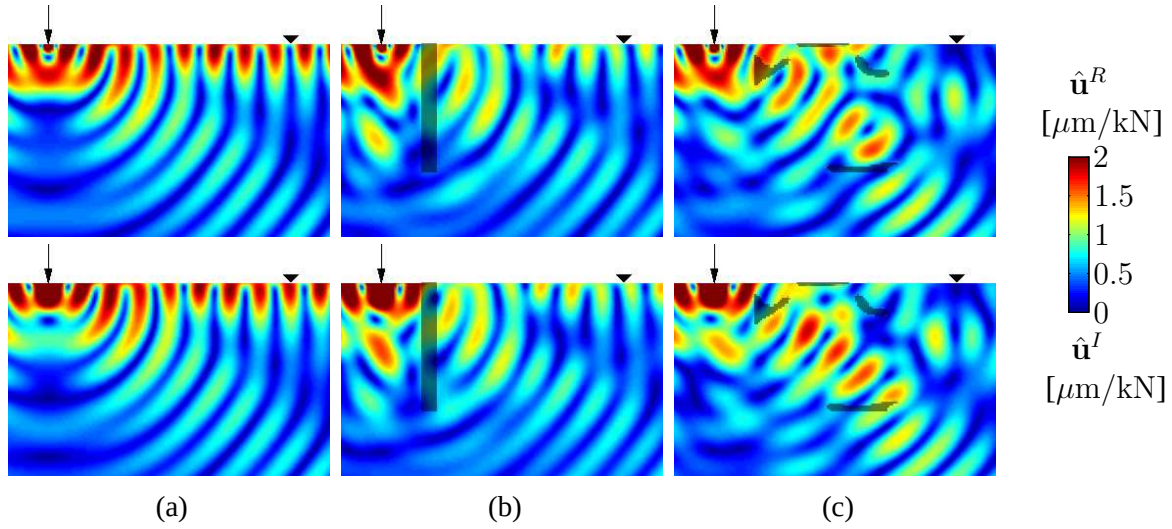

(a) (b) (c)

Figure 5: Vector norm of the real part $\hat{\mathbf{u}}^R$ (top) and imaginary part $\hat{\mathbf{u}}^I$ (bottom) of the displacement field at $50\,\mathrm{Hz}$ (a) for the homogeneous halfspace and after the introduction of (b) the reference design (figure 4a), and (c) the optimized design maximizing the insertion loss IL at $50\,\mathrm{Hz}$ (figure 4b).

densities are projected to the stiffened material, and the dimensions of the stiffened material decrease, leading to so-called eroded designs.

A high value for the insertion loss is found for the value $\eta = 0.5$ (intermediate design). The performance is therefore very sensitive to thickness variations. For the dilated design ($\eta = 0.25$), a high performance is still obtained thanks to the top part of the design. This top part is, however, largely affected for the eroded design ($\eta = 0.75$). The upper value $\eta = 1$ removes all stiffened material from the design ($\hat{u}^{\mathrm{out}} = \hat{u}^{\mathrm{out}}_{\mathrm{orig}}$), and the insertion loss (Eq. (1)) becomes equal to zero.

In order to obtain a design which is less sensitive to this type of geometric imperfections, a robust topology optimization approach is used. The interval of the projection threshold is set to $[0.25, 0.75]$ and a worst case formulation is adopted. In the worst case formulation, the minimal insertion loss for different values of the projection threshold is maximized. The robust optimization problem is formulated as follows:

$$\begin{aligned} \min_{\rho_e} \quad & \max_{q} \left\{ \Phi\left(\bar{\rho}_e(\eta^q)\right) \right\}, \quad q = 1 \ldots Q \\ \text{s.t.} \quad & \sum_{e=1}^{N} v_e \bar{\rho}_e^i \leq V^*, \qquad e = 1 \ldots N \\ & 0 \leq \rho_e \leq 1, \qquad e = 1 \ldots N \end{aligned} \tag{9}$$

where Q is the number of values considered for the projection threshold η and $\bar{\rho}_e^i$ are the element densities of element e in the case of the intermediate design ($\eta = 0.5$).

Figure 7 shows the resulting robust design and insertion loss for $Q = 3$ equidistant values of the projection threshold η. The deterministic performance decreases from $50.1\,\mathrm{dB}$ to $40.6\,\mathrm{dB}$. The robust design is, however, less sensitive to thickness variations. There are some small peaks at $\eta = 0.25$, $\eta = 0.5$ and $\eta = 0.75$ but these are not as distinct as the peak at $\eta = 0.5$ in figure 6d. The insertion loss at a frequency of $50\,\mathrm{Hz}$ is therefore larger than $26.5\,\mathrm{dB}$ for the entire range $\eta = [0.25, 0.75]$.

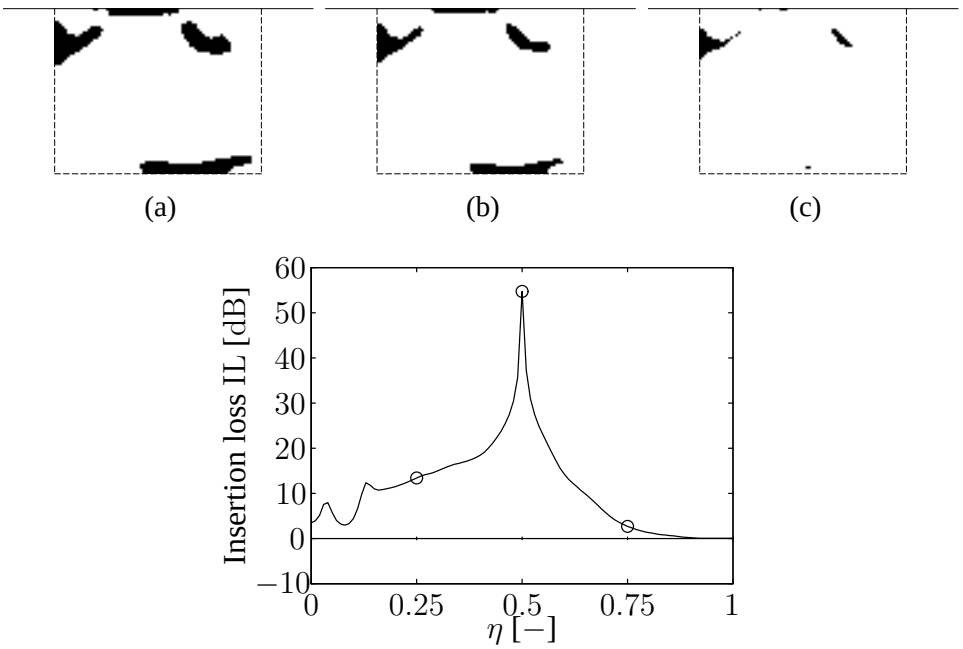

Figure 6: The (a) dilated ($\eta = 0.25$), (b) intermediate ($\eta = 0.5$), and (c) eroded ($\eta = 0.75$) version of the optimized design maximizing the insertion loss IL at a frequency of $50\,\mathrm{Hz}$ and (d) the influence of the projection threshold η on the insertion loss IL at $50\,\mathrm{Hz}$.

Because of buildability constraints, it may be difficult to reproduce the design in figure 7b. Since the design is robust to thickness variations, a simplification of the geometry is not expected to significantly affect the performance of the design. Figure 8 shows a manually simplified design and the corresponding insertion loss. The performance of this simplified design is similar to the performance of the design obtained with deterministic and robust topology optimization. The insertion loss at $50\,\mathrm{Hz}$ is equal to $33.0\,\mathrm{dB}$ and is therefore lower than the insertion loss of the robust design, but the simplified design still outperforms the reference design, which has an insertion loss equal to $4.4\,\mathrm{dB}$ at $50\,\mathrm{Hz}$.

5 CONCLUSIONS

Topology optimization is a powerful tool for finding novel design geometries. In this paper, topology optimization is used to design wave barriers that reduce ground transmission vibration. An optimization problem is considered where a homogeneous halfspace is excited at the surface. The response at a receiver point is minimized by stiffening material in the design domain between the source and receiver.

Harmonic excitation is considered and the optimized designs are shown at two frequencies ($25\,\mathrm{Hz}$ and $50\,\mathrm{Hz}$). At lower frequencies, the incoming waves are directed downwards away from the surface. At higher frequencies, destructive interference is observed, resulting in a peak at the targeted frequency.

Geometric imperfections can lead to an important deterioration of the performance. A worst case approach is therefore used to obtain a robust design, where the lowest performance of some values of the projection threshold is maximized. The resulting design is less sensitive to errors in the dimensions of the wave barrier. Simplifying the topology of the robust design leads to a

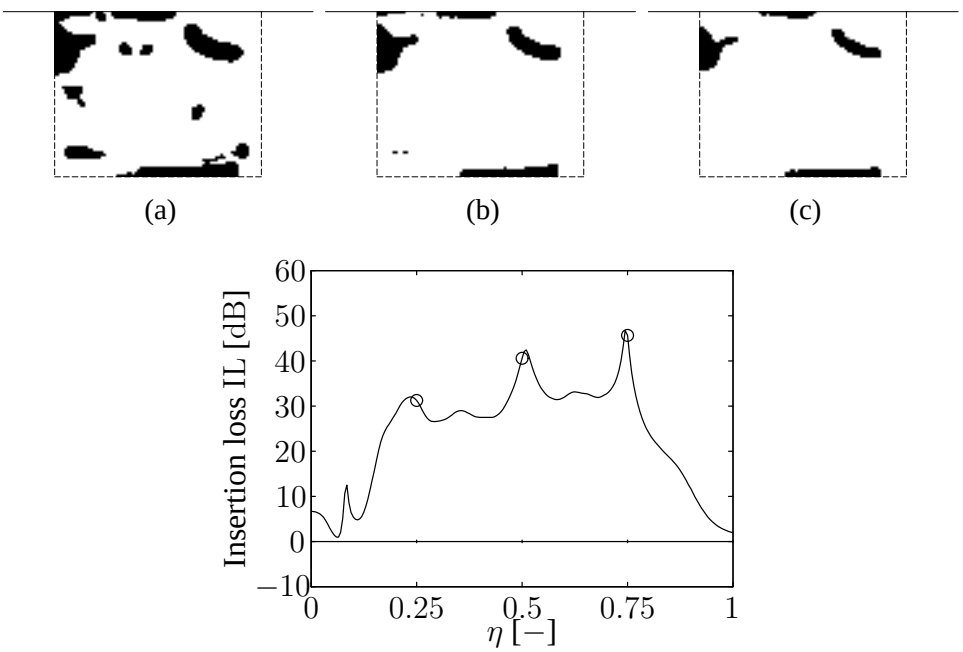

Figure 7: The (a) dilated ($\eta = 0.25$), (b) intermediate ($\eta = 0.5$), and (c) eroded ($\eta = 0.75$) version of the robust optimized design maximizing the minimal insertion loss IL for 3 equidistant values of the projection threshold η in the range $[0.25, 0.75]$ at a frequency of $50\,\mathrm{Hz}$ and (d) the influence of the projection threshold η on the insertion loss IL at $50\,\mathrm{Hz}$.

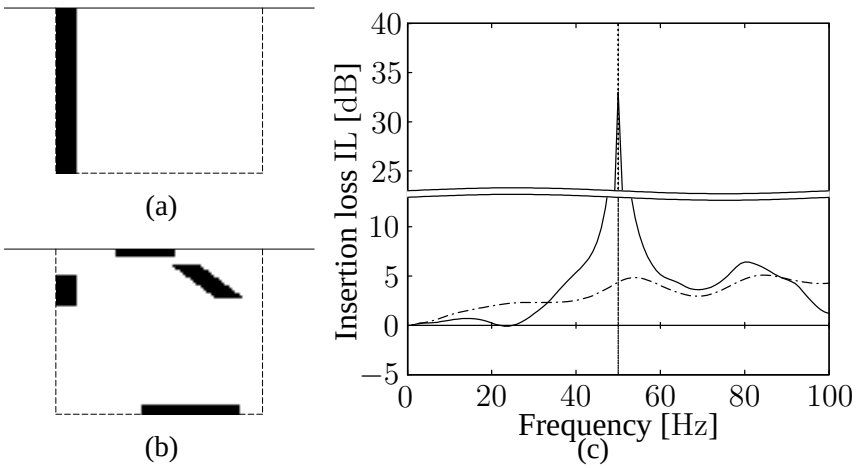

Figure 8: (a) Reference design, (b) simplified design after a manual post-processing of the robust optimized design maximizing the insertion loss at a frequency of $50\,\mathrm{Hz}$ using a worst case robust approach (figure 7b), and (c) resulting insertion loss IL as a function of the frequency for the reference design (dash-dotted line) and the post-processed optimized design (solid line).

slightly reduced performance, but the resulting design significantly outperforms the wall barrier.

ACKNOWLEDGEMENTS

The first author is a doctoral fellow of the Research Foundation Flanders (FWO). The financial support is gratefully acknowledged. The first, second and last authors are members of the KU Leuven-BOF PFV/10/002 OPTEC-Optimization in Engineering Center.

REFERENCES

[1] G. Lombaert, G. Degrande, B. Vanhauwere, B. Vandeborght, S. François, The control of ground-borne vibrations from railway traffic by means of continuous floating slabs. *Journal of Sound and Vibration*, **297**, 946–961, 2006.

[2] P. Coulier, S. François, G. Degrande, G. Lombaert, Subgrade stiffening next to the track as a wave impeding barrier for railway induced vibrations. *Soil Dynamics and Earthquake Engineering*, **48**, 119–131, 2013.

[3] J.P. Talbot, H.E.M. Hunt, A generic model for evaluating the performance of base-isolated buildings, *Journal of Low Frequency Noise, Vibration and Active Control*, **22**, 149–160, 2003.

[4] M.P. Bendsøe, O. Sigmund, *Topology optimization: theory, methods and applications*, Springer, Berlin, 2003.

[5] P. Borel, A. Harpøt, L. Frandsen, M. Kristensen, P. Shi, J. Jensen, O. Sigmund, Topology optimization and fabrication of photonic crystal structures, *Optic Express*, **12**, 1996–2001, 2004.

[6] O. Sigmund, J.S. Jensen, Systematic design of phononic band-gap materials and structures by topology optimization, *Philosophical Transactions of the Royal Society of London Series A: Mathematical, Physical and Engineering Sciences*, **361**, 1001–1019, 2003.

[7] M. Dühring, J. Jensen, O. Sigmund, Acoustic design by topology optimization, *Journal of Sound and Vibration*, **317**, 557–575, 2008.

[8] J. Kook, K. Koo, J. Hyun, J. Jensen, S. Wang, Acoustical topology optimization for Zwickers loudness model – Application to noise barriers, *Computer Methods in Applied Mechanics and Engineering*, **237**, 130–151, 2012.

[9] M. Jansen, G. Lombaert, M. Schevenels, Robust topoplogy optimization of structures with imperfect geometry based on geometric nonlinear analysis. *Computer Methods in Applied Mechanics and Engineering*, **285**, 452–467, 2015.

[10] I. Harari, U. Albocher, Studies of FE/PML for exterior problems of time-harmonic elastic waves. *Computer Methods in Applied Mechanics and Engineering*, **195**, 3854–3879, 2006.

[11] S.S. Kristensen, *Topology optimization for damping of ground vibration*, Master's thesis, DTU, 2012.

[12] J.K. Guest, J.H. Prévost, T. Belytschko, Achieving minimum length scale in topology optimization using nodal design variables and projection functions. *International Journal for Numerical Methods in Engineering*, **61**, 238–254, 2004.

[13] K. Svanberg, The method of moving asymptotes – a new method for structural optimization. *International Journal for Numerical Methods in Engineering*, **24**, 359–373, 1987.

[14] M. Schevenels, B.S. Lazarov, O. Sigmund, Robust topology optimization accounting for spatially varying manufacturing errors. *Computer Methods in Applied Mechanics and Engineering*, **200**, 3613–3627, 2011.